CrossMark

ORIGINAL PAPER

Dynamic Analysis of a Twin Tunnel in Soil Subjected to Internal Blast Loading

Rohit Tiwari[1] · Tanusree Chakraborty[1] · Vasant Matsagar[1]

Abstract The present study deals with three-dimensional (3-D) nonlinear finite element analyses of a twin tunnel in soil with reinforced concrete (RC) lining subjected to internal blast loading. Blast load has been simulated using the coupled Eulerian Lagrangian (CEL) analysis tool available in finite element software Abaqus/Explicit. Soil mass and RC lining have been modeled using 3-D eight node reduced integration Lagrangian elements (C3D8R). Beam elements (B31) have been used to model reinforcement of RC lining. A 50 kg trinitrotoluene (TNT) charge weight has been used in the analysis. Eight node reduced integration Eulerian elements (EC3D8R) have been used for modeling TNT explosive and surrounding air. Drucker–Prager plasticity model have been used to simulate strain rate dependent behavior of soil mass. For simulating strain rate dependent behavior of concrete and steel, concrete damaged plasticity and Johnson–Cook (J–C) plasticity models have been used, respectively. The explosive TNT has been modeled using Jones–Wilkins–Lee (JWL) equation of state. Investigations have been performed for studying the deformation, damage of RC lining and surrounding soil mass. Pressure in the RC lining and surrounding soil mass, caused by explosive induced shock wave has been studied for both tunnels. It is observed that damage and deformation of RC lining and soil mass are dependent on charge weight and clearance between the tunnels.

Introduction

Tunnels are important infrastructure in any modern metropolis. In order to safeguard traffic tunnels from fanatic activities, e.g. terrorist attack and accidental events, it is necessary to design the tunnels in such a way that the structure undergoes minimum damage and can be brought back to functionality with minimal repair and in minimum time when subjected to an extreme unforeseen load such as blast. Blast resistant design of tunnel requires that the response of the tunnels subjected to blast loading are understood in-depth through advanced numerical modeling.

Numerical analysis of tunnel subjected to blast loading has been reported in the literature by several researchers. Chille et al. [8] investigated dynamic response of an underground electric power plant subjected to internal explosive loading using three-dimensional (3-D) numerical analysis procedures. Coupled fluid–solid interaction was considered in their study, however, the nonlinearity and failure behavior of rock and concrete as well as the inter-action between different solid media were not simulated. Choi et al. [9] used 3-D finite element (FE) method and coupled fluid–solid interaction to study the blast pressure and resulting deformation in concrete lining for traffic tunnels in rock. They reported that the blast pressure on tunnel lining was not the same as the normally reflected pressure obtained using conventional weapons (CONWEP)

✉ Tanusree Chakraborty
   tanusree@civil.iitd.ac.in

   Rohit Tiwari
   rohit19862009@gmail.com

   Vasant Matsagar
   matsagar@civil.iitd.ac.in

1 Department of Civil Engineering, Indian Institute of Technology (IIT) Delhi, Hauz Khas, New Delhi 110 016, India

[29]. Lu [26], Gui and Chien [16] and Liu [25] used FE procedure to perform blast analysis of tunnels in soil subjected to external blast loading and reported stresses and deformation in tunnel. However, they did not consider high strain rate behavior of soil. Also, blast load was simulated using CONWEP. Feldgun et al. [13, 14] and Karinski et al. [19] used the variational difference method to analyze tunnel and cavities subjected to blast loads. Yang et al. [32] studied response of metro tunnel subjected to above ground explosion through finite element analysis procedure and von-Mises material model for soil. Liu [24] performed finite element analysis of tunnel with cast-iron lining subjected to blast loading simulated using CONWEP. Higgins et al. [17] carried out plain strain analysis of tunnel in sand subjected to internal blast loading considering high strain rate stress–strain response of soil using a bounding surface plasticity constitutive model. However, their study assumed elastic stress–strain response for concrete lining in the tunnel. Chakraborty et al. [6] compared the performance of steel and concrete conventional tunnel linings with sandwich panel linings made up of shock absorbing foam material as the core of the sandwich panels in tunnel subjected to blast loading. The blast load was calculated through a coupled fluid dynamics simulation and applied as a pressure pulse on the tunnel lining. Kumar et al. [20] studied the response of semi-buried structures under blast loading. In their analyses, the blast load was simulated using pressure pulse and soil stress–strain response was simulated using springs. However, advanced three-dimensional (3-D) nonlinear dynamic analyses of two tunnels adjacent to each other in soil with reinforced concrete (RC) tunnel lining, rigorous modeling of the reinforcement cage inside the lining, properly simulated explosive load using Jones–Wilkins–Lee (JWL) equation of state (EOS), interaction between explosive cloud and the surrounding lining and soil are rather unavailable in the literature due to extremely challenging nature of the problem.

The specific objectives of the present study are (1) to perform 3-D nonlinear dynamic finite element (FE) analysis of twin tunnels where blast happens inside one of the tunnels and (2) to understand the response of tunnel linings and surrounding soil when subjected to blast load. The tunnel in which blast occurs has been named in the present study as donor tunnel and the other tunnel is named as receiver tunnel. The FE analyses are performed using the commercially available FE software Abaqus version 6.11 (Abaqus manual version 6.11) through the coupled Eulerian Lagrangian (CEL) modeling technique. The soil and RC lining of the twin tunnels are modeled using the Lagrangian elements. The trinitrotoluene (TNT) explosive and surrounding air has been modeled using the Eulerian elements. Blast loading may generate up to 10^4/s strain rate in any material [11, 28]. Hence, strain rate dependent material properties have been

used for all the materials used in the present simulations. Soil stress–strain response is simulated using the Drucker–Prager constitutive model [23, 25]. The stress–strain response of concrete lining is simulated using the concrete damaged plasticity model [6]. The stress–strain behavior of steel reinforcement is simulated using the Johnson–Cook (J–C) plasticity model [18]. The pressure–volume relationship of the explosive is simulated using the JWL EOS. The analysis results have been studied for deformation of the RC lining and soil and pressure on the lining.

Three-Dimensional Finite Element Modeling

Lagrangian Finite Element Modeling of Soil and RC Lining

The 3-D FE model of the twin tunnel in soil is developed using Abaqus (version 6.11) software with the Lagrangian analysis option. The FE mesh of the soil, tunnel lining and reinforcement inside the lining are shown in Fig. 1a through e. A 20 m long tunnel geometry with 350 mm thick RC lining has been prepared in soil with the central axis of the tunnel placed at a depth of 7.5 m from the ground surface. The steel reinforcement has been modeled with 10 and 12 mm diameter bars in longitudinal and hoop reinforcement directions, respectively. The hoop reinforcement rings are placed at 250 mm centre-to-centre spacing. The longitudinal reinforcement bars are placed at a distance of 850 mm centre-to-centre. Two layers of hoop reinforcement have been placed with 120 mm distance between the inner and the outer hoop reinforcement rings. The 20 m long tunnels are placed in a soil domain of 20 m long and 20 m × 15 m cross-section [10]. The FE models of the soil and concrete lining are developed in Abaqus/CAE using the 3-D part option and eight node brick element (C3D8R) with reduced integration, hourglass control and finite membrane strains. Mesh convergence and boundary convergence studies have been performed and higher mesh density has been used in tunnel lining and soil close to the lining for achieving higher accuracy. The steel reinforcement has been embedded using the two node beam elements (B31). Proper bonding between concrete and reinforcement bars is assured by embedding the reinforcement bars in the RC linings. The contact between tunnel linings and soil is modeled with the general contact option in Abaqus with hard contact in normal direction and frictionless contact in tangential direction. Among the boundary conditions, the bottom plane of the soil domain is fixed in all Cartesian directions, e.g. x, y and z. The vertical side planes and the front and back side planes of the soil domain and the lining have been provided with partially fixed supports as detailed in Fig. 1a by constraining the

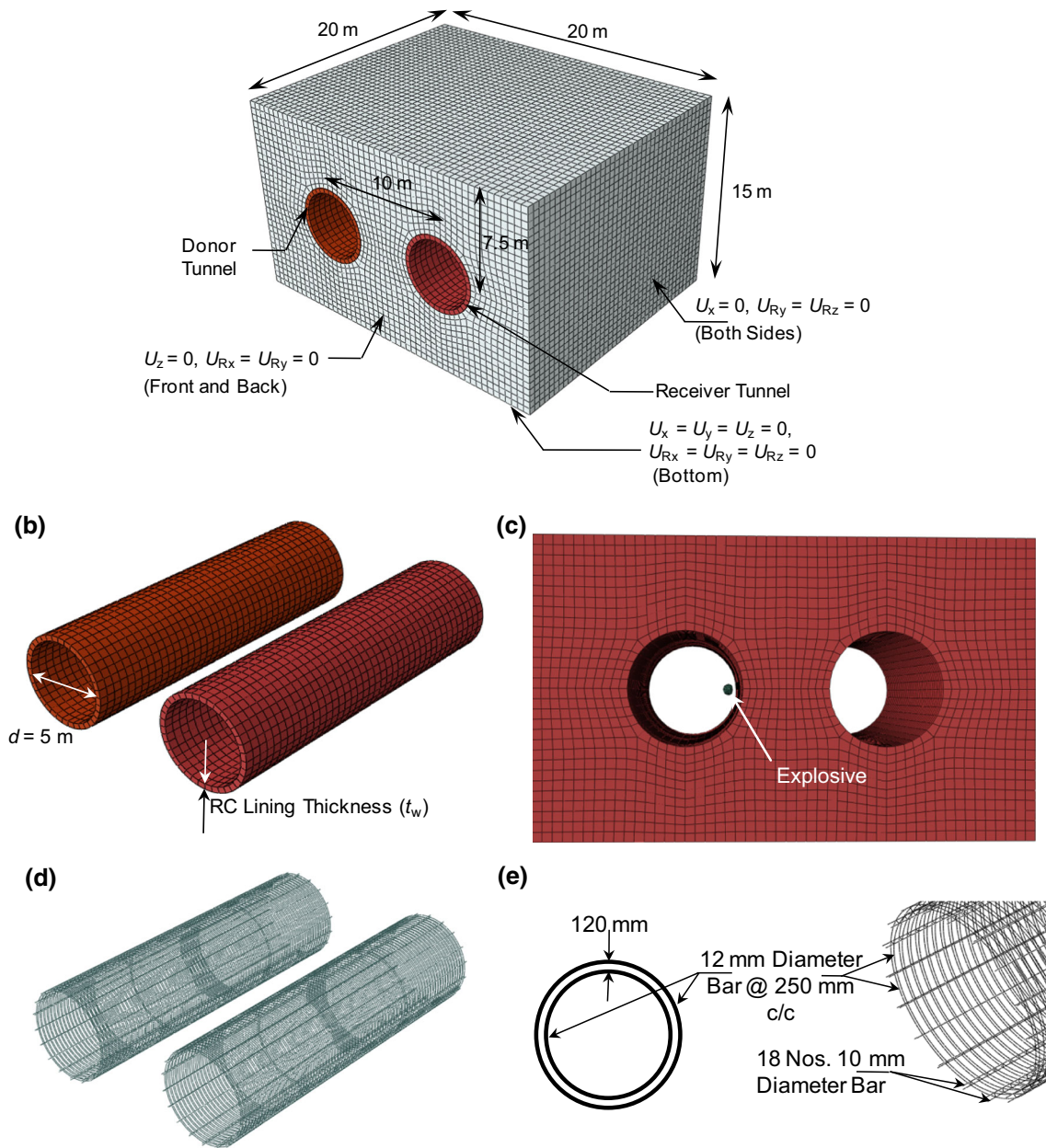**(a)** Typical geometry, mesh and boundary conditions for twin tunnels in soil

Fig. 1 Twin tunnels geometry, explosive location and reinforcement details

normal displacements perpendicular to the plane (U_x, U_y and U_z) and the out of plane rotations (U_{Rx}, U_{Ry} and U_{Rz}).

Eulerian Finite Element Modeling of Explosive

The explosive material has been modeled using the Eulerian modeling technique in Abaqus. Figure 1c shows the location of TNT explosive inside the tunnel. In Abaqus coupled Eulerian Lagrangian (CEL) modeling option, the Eulerian material flows through the Lagrangian structure. Thus, the simulation that generates a large amount of deformation and

stress in the elements and results in an error or inaccuracy in the Lagrangian analysis may be successfully carried out using the CEL tool. Herein, Eulerian continuum 3-D eight node reduced integration elements (EC3D8R) are used [1] to model Eulerian explosive material and the surrounding air domain inside the tunnel. These Eulerian elements may be completely or partially filled by explosive material, while the rest of the Eulerian grid is void. In Eulerian analysis, the material is tracked by means of Eulerian volume fractions (EVF) when it flows through the mesh. The EVF represents the ratio by which each Eulerian element is filled with

material; i.e. EVF = 1 representing element completely filled with material and EVF = 0 representing completely void elements. The boundary of Eulerian material may not match the element geometry during the analysis and has to be recomputed at each time instant as the material flows through the mesh. Dimensions of the grid containing Eulerian elements are taken sufficiently large to prevent the loss of air from the Eulerian grid after blast as this would have lead to artificial loss of kinetic energy, consequently reducing the accuracy of the obtained results. The Eulerian and Lagrangian elements can interact with each other through the general contact option defined between explosive, air and tunnel lining surfaces. Free outflow boundary condition has been defined at the boundary of the air domain. Thus, the blast pressure when reaches the boundaries of air domain, propagates freely out of the air domain without any kind of reflection. A fine mesh of Eulerian elements is necessary to efficiently capture the propagation of blast wave through air and through the surrounding concrete lining and soil. The mesh convergence study has been performed in the present study to decide the smallest element size.

The pressure (p) for the TNT explosive can be calculated using Jones–Wilkins–Lee (JWL) equation of state (EOS) [21] given by

$$p = A\left(1 - \frac{\omega}{R_1\bar{\rho}}\right)e^{-R_1\bar{\rho}} + B\left(1 - \frac{\omega}{R_2\bar{\rho}}\right)e^{-R_2\bar{\rho}} + \omega\rho e_{int} \quad (1)$$

where A, B, R_1, R_2 and ω are material constants for TNT explosive. Parameters A and B represent the magnitudes of pressure, $\bar{\rho}$ is the ratio of the density of the explosive in the solid state (ρ_{sol}) to the current density (ρ) and e_{int} is the specific internal energy at atmospheric pressure. In the JWL equation of state, the first two exponential terms on the right hand side represent high pressure generated during explosion and the last term on right hand side is a low pressure term which deals with high volume due to explosion. The material properties used herein for the JWL EOS are listed in Table 1.

Constitutive Models of Materials

Constitutive Model of Concrete

Concrete in RC lining has been modeled as M30 grade (maximum compressive strength 30 MPa) using concrete

damaged plasticity model in Abaqus. The stress–strain relation of concrete damaged plasticity model is given by

$$\sigma_t = (1 - d_t)D_0^{el} : \left(\varepsilon - \varepsilon_t^{pl}\right) \quad (2)$$

$$\sigma_c = (1 - d_c)D_0^{el} : \left(\varepsilon - \varepsilon_c^{pl}\right) \quad (3)$$

where t and c represent tension and compression behavior, respectively. Here, σ_t and σ_c are tensile and compressive stress vectors, respectively; ε_t^{pl} and ε_c^{pl} are plastic strains; d_t and d_c are the damage variables which are considered functions of plastic strain; D_0^{el} is the undamaged initial elastic modulus. The yield function in the considered damaged plasticity model is given by Lubliner et al. [27] and later modified by Lee and Fenves [22], given by

$$F = \left(\sqrt{3/2}\sqrt{\bar{s}:\bar{s}}\right) - 3\alpha\bar{p} + \beta\langle\hat{\bar{\sigma}}_{max}\rangle - \gamma\langle-\hat{\bar{\sigma}}_{max}\rangle$$
$$- (1 - \alpha)\bar{\sigma}_c = 0 \quad (4)$$

where

$$\alpha = \frac{(\sigma_{b0}/\sigma_{c0}) - 1}{2(\sigma_{b0}/\sigma_{c0}) - 1} \quad (5)$$

$$\beta = \frac{\bar{\sigma}_c}{\bar{\sigma}_t}(1 - \alpha) - (1 + \alpha) \quad (6)$$

$$\gamma = \frac{3(1 - K_c)}{2K_c - 1} \quad (7)$$

$$\bar{\sigma}_c = \frac{\sigma_c}{(1 - d_t)} \quad (8)$$

$$\bar{\sigma}_t = \frac{\sigma_t}{(1 - d_t)} \quad (9)$$

where $\hat{\bar{\sigma}}_{max}$ is the maximum principal effective stress; $\bar{s}$ is the deviatoric stress tensor; σ_{b0}/σ_{c0} is the ratio of initial equibiaxial compressive yield stress to initial uniaxial compressive yield stress; d_t is the damage variable and K_c is the ratio of the second deviatoric stress invariant on the tensile meridian to that on the compressive meridian at initial crushing for any given value of effective mean stress, $\bar{p} = (\bar{\sigma}_1 + \bar{\sigma}_2 + \bar{\sigma}_3)/3$.

The concrete damaged plasticity model assumes a non-associated plastic flow. The plastic potential function G_p used for this model is given by

$$G_p = \sqrt{(\varepsilon\sigma_{t0}\tan\psi)^2 + \left(\frac{3}{2}s:s\right)} - \bar{p}\tan\psi \quad (10)$$

Table 1 JWL material properties for TNT explosive [21]

Density (ρ_{sol}) (kg/m³)	Detonation wave speed (v_{det}) (m/s)	A (MPa)	B (MPa)	ω	R_1	R_2	Detonation energy density (e_{int}) (kJ/kg)
1630	6930	373,800	3747	0.35	4.15	0.9	3680

where ψ is the dilation angle at mean stress–deviatoric stress plane; σ_{t0} is the uniaxial tensile stress at failure, value of which is set by the user and ε is the eccentricity parameter. If the eccentricity is zero plastic potential function becomes straight line. In the present study, elastic material properties and compressive strength of concrete are presented in Table 2. Figure 2a, b show the stress–strain curves for M30 concrete in compression and tension, respectively [4, 5]. Figure 2c, d show the damage density-strain curves for M30 concrete in compression and tension, respectively [2]. Damage density is defined as the ratio of the total damaged area to the whole cross sectional area; damage density value is varied from 0 to 1, damage density 0 means the material is undamaged and damage density 1 means the material is completely damaged. The strain rate dependent strength properties of concrete and the dynamic increment factor (DIF) under compressive and tensile loading are obtained from Bischoff and Perry [3]. Herein, DIF values of 2.1 and 6 at 100/s strain rate have been used on the static compressive and tensile strength values of concrete, respectively.

Constitutive Model of Steel

The stress–strain behavior of steel reinforcement has been modeled using Johnson–Cook (J–C) model [18]. The dynamic yield stress (σ)-strain (ε) relationship of the J–C model is given by

$$\sigma = (A + B\varepsilon^n)(1 + C\log_e \varepsilon^*)(1 - T^{*m}) \quad (11)$$

where ε^* is dimensionless plastic strain; $\varepsilon^* = \dot{\varepsilon}/\dot{\varepsilon}_0$ in which $\dot{\varepsilon}$ is the equivalent plastic strain rate and $\dot{\varepsilon}_0 = 1/s$ is reference strain rate. Here, A, B, C, m and n are the model parameters; T^* is the homologous temperature. In the present study, temperature dependence of material stress–strain response has not been considered. For steel, the density ρ, elastic modulus E, Poisson's ratio υ and tensile yield strength f_s are given in Table 3. For strain rate dependent modeling using the J–C model, the material constants A, B, C and n were obtained from mechanical testing neglecting the temperature effects and adopted herein for strain rate of 100/s as given in Table 3 [15].

Constitutive Model of Soil

The stress–strain response of soil has been simulated using the Drucker–Prager plasticity model. The yield criterion of the Drucker–Prager model is given by

$$F = \frac{q}{2}\left[1 + \frac{1}{K} - \left(1 - \frac{1}{K}\right)\left(\frac{r}{q}\right)^3\right] - p'\tan\beta - d = 0 \quad (12)$$

where q is the deviatoric stress $\left[= \sqrt{3/2}\sqrt{s_{ij} : s_{ij}}\right]$, s_{ij} is the deviatoric stress tensor, p' is the mean stress $= (\sigma_1' + \sigma_2' + \sigma_3')/3$, K is a scalar parameter that determines the shape of the yield surface and maintains the convexity of the yield surface in the deviatoric (π) plane, r is the third invariant of the deviatoric stress tensor. The parameter β is related to the angle of internal friction ϕ at the stage of no dilatancy (the critical state of sand) using a correlation given by

$$\tan\beta = \frac{\sqrt{3}\sin\phi}{\sqrt{1 + (1/3)\sin^2\phi}} \quad (13)$$

and d is the hardening parameter related to cohesion, c through a correlation given by

$$\frac{d}{c} = \frac{\sqrt{3}\cos\phi}{\sqrt{1 + (1/3)\sin^2\phi}}. \quad (14)$$

For sands, the cohesion (c) is considered to be zero. The plastic potential surface, G_P of the model is given by

$$G_P = \frac{q}{2}\left[1 + \frac{1}{K} - \left(1 - \frac{1}{K}\right)\left(\frac{r}{q}\right)^3\right] - p'\tan\psi_{tp} \quad (15)$$

where ψ_{tp} is related to the dilatancy angle, ψ through a correlation given by

$$\tan\psi_{tp} = \frac{\sqrt{3}\sin\psi}{\sqrt{1 + (1/3)\sin^2\psi}}. \quad (16)$$

A non-associated flow rule is considered in the present analysis by considering the dilatancy angle of sand to be different from the angle of internal friction. For sand, the density, elastic material properties, angle of internal friction and dilation angle are presented in Table 4. The strain rate dependent stress–strain response of sand has been obtained from [31]. Figure 3 shows the stress–strain relationship of Ottawa sand at 1000/s strain rate as obtained from Veyera and Ross [31].

Types of Analyses

To ensure the validity of the present numerical simulations the results of CEL analyses of blast loading on a concrete slab have been compared with (1) the analysis results when blast loading is simulated using a pressure pulse calculated using UFC 3-340-02 manual and the modified Friedlander's Eq. (2) numerical simulation results collected from

Table 2 Material properties for concrete

Density (ρ_c) (kg/m³)	Poisson's ratio (v_c)	Elastic modulus (E_c) (GPa)	Compressive strength (f_{ck}) (MPa)
2400	0.2	27.4	30

Fig. 2 Static stress–strain and damage–strain curves for M30 grade of concrete under compression and tension at 100/s strain rate [2, 4, 5]
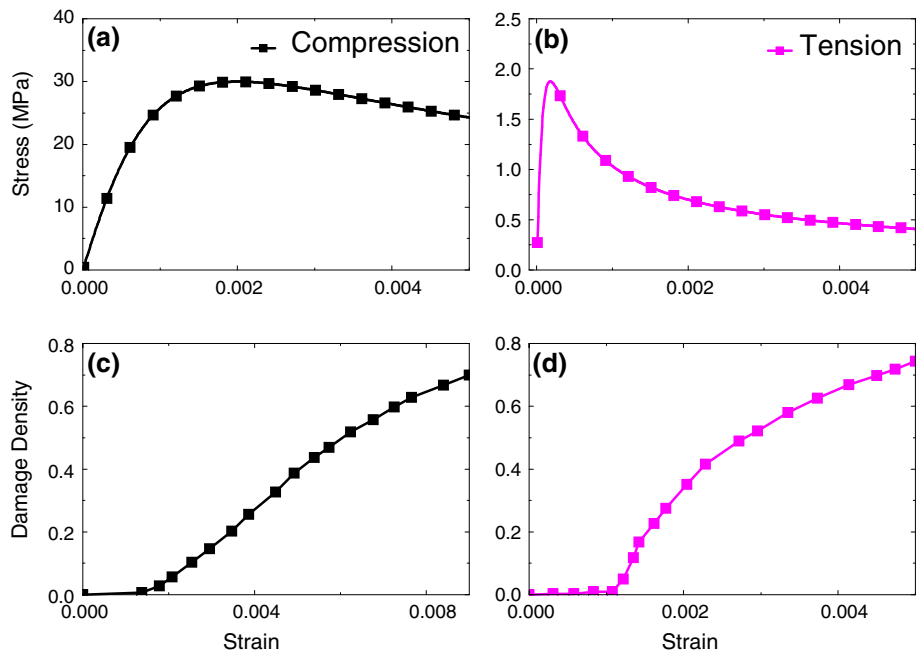

Table 3 Material properties for steel

Density (ρ_s) (kg/m^3)	Poisson's ratio (v_s)	Elastic modulus (E_s) (GPa)	Tensile yield strength (f_s) (MPa)	A (MPa)	B (MPa)	n	C
7800	0.3	210	300	360	635	0.114	0.075

Table 4 Material properties for sand

Density (ρ_{sand}) (kg/m^3)	Poisson's ratio (v_{sand})	Elastic modulus (E_{sand}) (GPa)	Angle of internal friction (ϕ) (°)	Dilation angle (ψ) (°)
1560	0.2	0.028	30	5

Du and Li [12] and (3) results of experimental investigation carried out by Zhao and Chen [33]. The analysis has been performed in the single step using the dynamic explicit module available in Abaqus. Explosive weight of 50 kg is used in the numerical simulations. Thickness of RC lining (t_w) is maintained at 350 mm in all cases.

Solution Scheme

The dynamic explicit analyses in the CEL approaches have been performed using central difference integration scheme in single step. This scheme uses a time increment (Δt) that is smaller than the Courant time limit, $\Delta t \leq l/c$, where l is the smallest element dimension and c is the speed of sound wave in the medium in which it travels. For studying the response of complete 20 m tunnel section, the duration of analysis is maintained at 26 millisecond (ms)
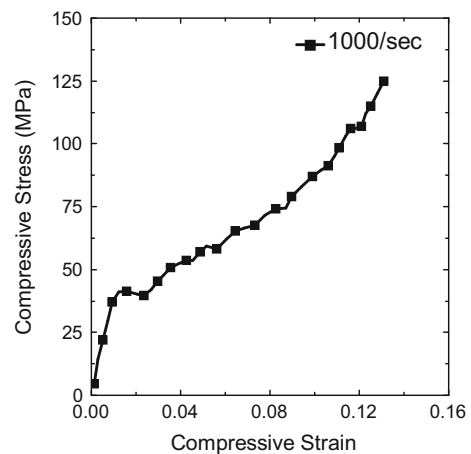

Fig. 3 Stress–strain curve for Ottawa sand at 1000/s strain rate [31]

such that the shock wave can travel through the complete length of the tunnel. In order to properly represent the propagation of the blast induced compressive stress wave, artificial bulk viscosity is activated by employing quadratic and linear functions of volumetric strain rates with default values of 1.2 and 0.06, respectively [1].

## Validation of FE Model and CEL Procedure

Validation for Capability of JWL EOS in Blast Simulation

Herein, a 1.2 m × 1.2 m × 90 mm concrete slab subjected to a blast load caused by 1.69 kg TNT charge weight (W) at three different scaled distances of 0.5, 1 and 2 m/kg$^{1/3}$ has been analyzed numerically using the CEL method. In the CEL method, the TNT explosive has been simulated using the JWL EOS. The M25 concrete has been modeled with a compressive strength of 25 MPa, mass density of 2500 kg/m^3, Young's modulus of 25 GPa and Poisson's ratio of 0.2. The boundaries of the concrete slab are restrained in all three Cartesian directions, e.g. x, y and z. In another set of analysis, the blast load is calculated using the UFC 03-340-02 manual and the modified Friedlander's equation for the same scaled distances mentioned above and the same charge weight of 1.69 kg. Figure 4a through c show the comparison of central node displacement of the concrete slab calculated from the analysis results using the JWL model and its comparison with the results obtained from the simulation using UFC 03-340-02. From Fig. 4 it is observed that the results obtained from both the analyses compare with reasonable accuracy. Figure 5a through c show the pressure time histories calculated using JWL EOS. The peak pressure values are compared with the pressure magnitudes obtained from UFC 3-340-02 manual. Both the pressure values are observed to be in close agreement.

Validation for Blast Analysis using JWL with the Numerical Analysis Results

The validity of the current modeling approach using the CEL method and JWL EOS for explosive is also ensured by comparing the simulation results with the numerical simulation results collected from Du and Li [12]. They analyzed dynamic behavior of RC slabs under blast loading. A RC slab of size 2 m × 1 m × 100 mm is used in these analyses. The slab has been reinforced with 10 and 12 mm diameter bars with 100 mm centre-to-centre spacing, in both directions placed at mid-depth. A charge weight of 1000 kg TNT was placed at a stand-off distance of 10 m from the centre of the slab. The boundaries of the concrete slab are restrained in three Cartesian directions, e.g. x, y and z. The FE software LS-Dyna was used for the analysis performed by Du and Li [12]. The Johnson–Holmquist material model was used to simulate concrete stress–strain response whereas the Cowper and Symond's model was used for steel. In the present study, the RC slab model with the same explosive charge weight and scaled distances as considered by Du and Li [12] is prepared using the CEL procedure. The JWL EOS has been used to model explosive material. The material properties of steel and concrete have been considered to be the same as that assumed by Du and Li [12]. Concrete damaged plasticity model has been used to simulate the stress–strain response of concrete whereas von-Mises model has been used for

Fig. 4 Comparison of central node displacement time histories for simulations using JWL EOS and pressure time history calculated from UFC 3-340-02 and modified Friedlander's equation
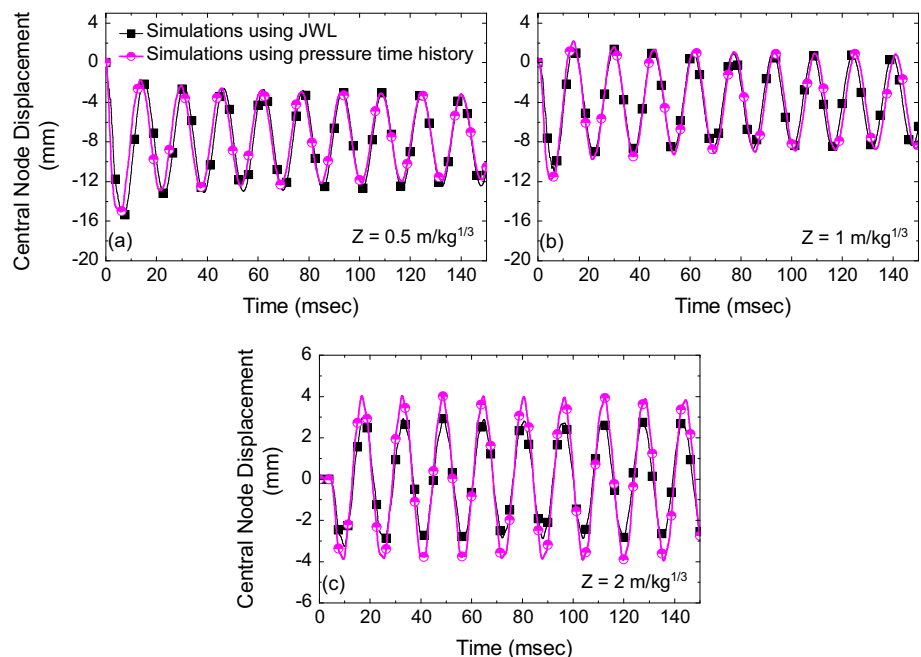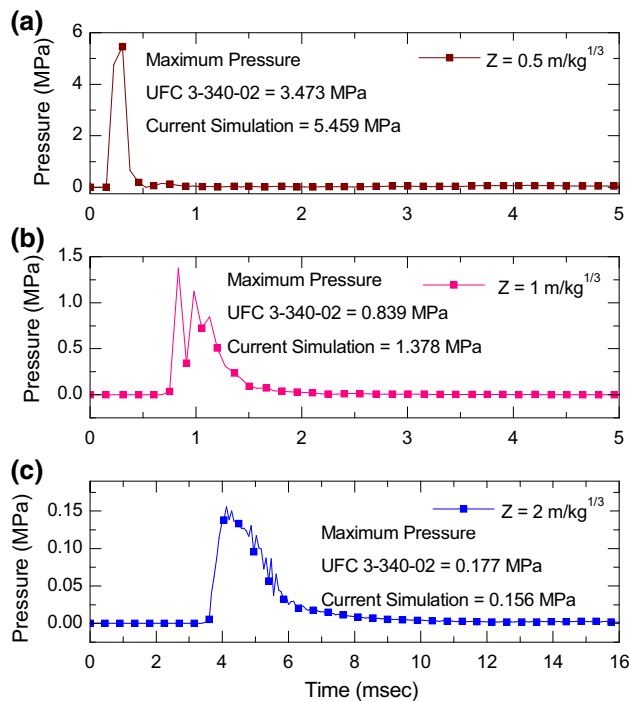
Fig. 5 Pressure time histories obtained from CEL simulations using JWL EOS and comparison of peak pressure obtained from UFC 3-340-02
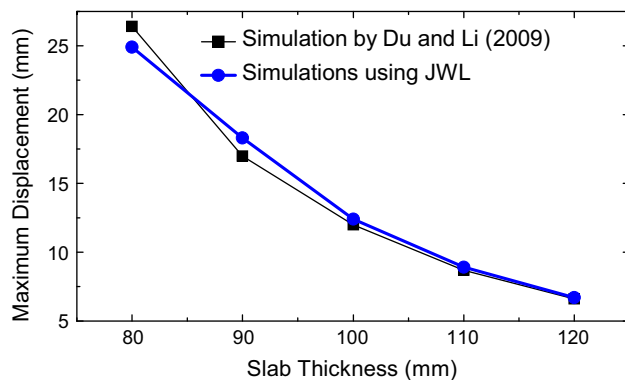

Fig. 6 Variation of maximum displacement for different concrete slab thicknesses obtained from CEL simulations using JWL EOS with the results reported by Du and Li [12]

steel. The concrete in RC slab has been modeled with a compressive strength of 23.7 MPa, mass density of 2400 kg/m^3, shear modulus of 12.7 GPa and Poisson's ratio of 0.2 as mentioned in Du and Li [12]. Steel in RC slab has been modeled with yield strength of 335 MPa, mass density of 7800 kg/m^3, Young's modulus of 207 GPa and Poisson's ratio of 0.3. Figure 6 shows the maximum displacement of the concrete slab when subjected to blast load for different slab thicknesses. The current simulation results compare with that from the literature with

reasonable accuracy duly validating the CEL method based simulation procedure adopted herein.

Validation for Blast Analysis using JWL with the Experimental Data

The CEL simulation results have also been compared with experimental data for different charge weights, e.g. 0.2, 0.31 and 0.46 kg placed at a stand-off distance of 400 mm from the centre of slab as reported by Zhao and Chen [33]. A RC slab of size 1 m × 1 m × 40 mm has been used for the analyses. The RC slab has been reinforced with 6 mm diameter bars, spaced at 75 mm centre-to-centre in both directions. The boundaries of the RC slab are restrained in three Cartesian directions, e.g. x, y and z along two sides. In the present study, a similar model has been prepared using the CEL procedure and the charge weights as considered by Zhao and Chen [33] are taken. The material properties of steel and concrete have been considered to be the same as assumed by Zhao and Chen [33]. Concrete in RC slab has been modeled with a compressive strength of 39.5 MPa and Young's modulus of 28.3 GPa. Steel in RC slab has been modeled with yield strength of 600 MPa and Young's modulus of 200 GPa. Concrete damaged plasticity model has been used for concrete whereas von-Mises model has been used for steel. Table 3 shows the central node displacement of the concrete slab under blast load for different slab thicknesses. Reasonable agreement of the current simulation results with experimental and numerical investigations reported by Zhao and Chen [33] is observed in Table 5.

Results and Discussion on Parametric Studies

Numerical investigations for twin tunnels in soil are carried out to understand the response of twin tunnels when one tunnel is subjected to blast load. Figure 7 shows the various paths considered along the RC lining and the surrounding soil. Herein, tensile stresses are considered positive and displacement values in the direction of the positive x, y and z axes are considered positive.

Figure 8 shows the x directional (horizontally across the cross-section) displacement of the RC lining and the surrounding soil along the path defined at their side walls at 26 ms. It is observed from Fig. 8a that the RC lining and surrounding soil of the donor tunnel with explosive placed near to its RC lining shows higher displacement. The RC lining of donor tunnel shows a maximum displacement of 135 mm at the middle of tunnel right side wall. Soil surrounding the RC lining of the donor tunnel shows a maximum displacement of 284 mm near the middle of tunnel right side wall. Figure 8b shows the x directional displacement of RC lining and the surrounding soil of the receiver

Fig. 7 Paths defined for
visualization. Paths defined
along the tunnel **a** with
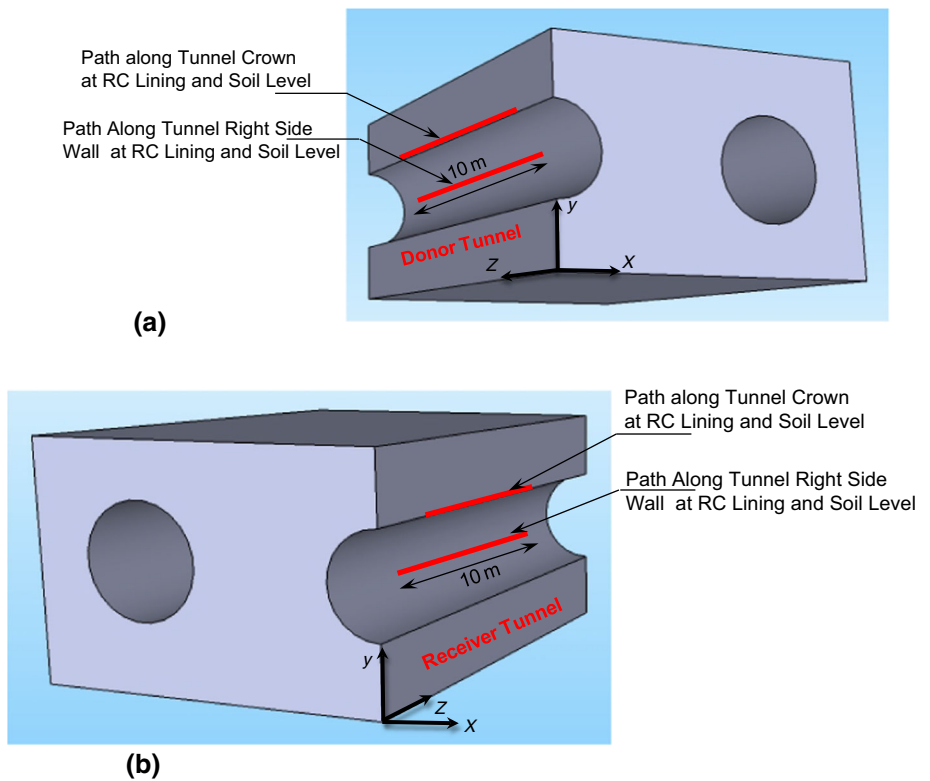explosive, **b** opposite to the
explosive

Table 5 Comparison of numerical simulation results with experimental data [33]

Charge weight (kg)	Central node displacement (mm)		
	Experiment by Zhao and Chen	Numerical simulation by Zhao and Chen	Numerical simulation in Present Study
0.2	10	8.8	7.7
0.31	15	12.7	13.2
0.46	35	31.1	29.5

Fig. 8 Displacement of RC
lining and surrounding soil at
26 ms
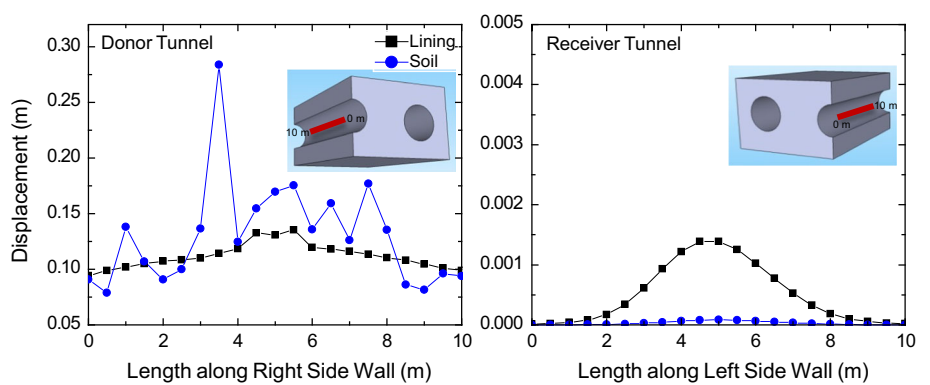
tunnel. The RC lining and surrounding soil of the receiver tunnel shows less displacement at its left side wall (towards the tunnel experiencing explosion). It is observed that due to attenuation of shock wave and particle rearrangement, left side wall of the receiver tunnel shows small displacement.

Figure 9 shows the y directional (vertically across the cross-section) displacement of soil from crown of the donor tunnel to ground level and x directional displacement of soil column between receiver and donor tunnel at 26 ms. It is observed that displacement of soil surrounding the RC
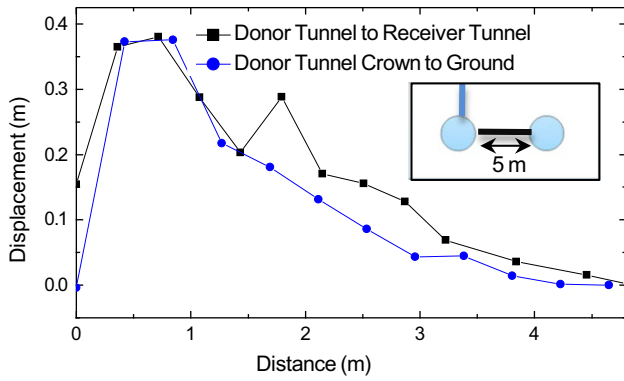
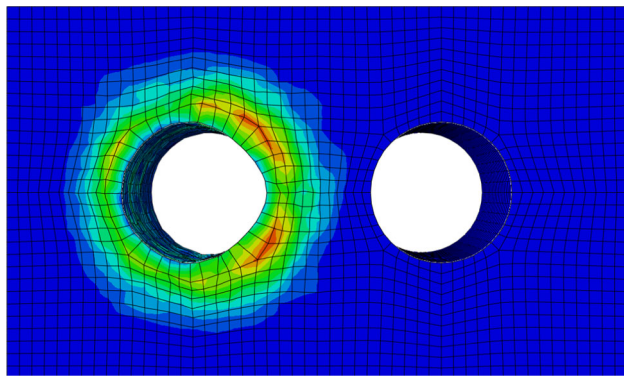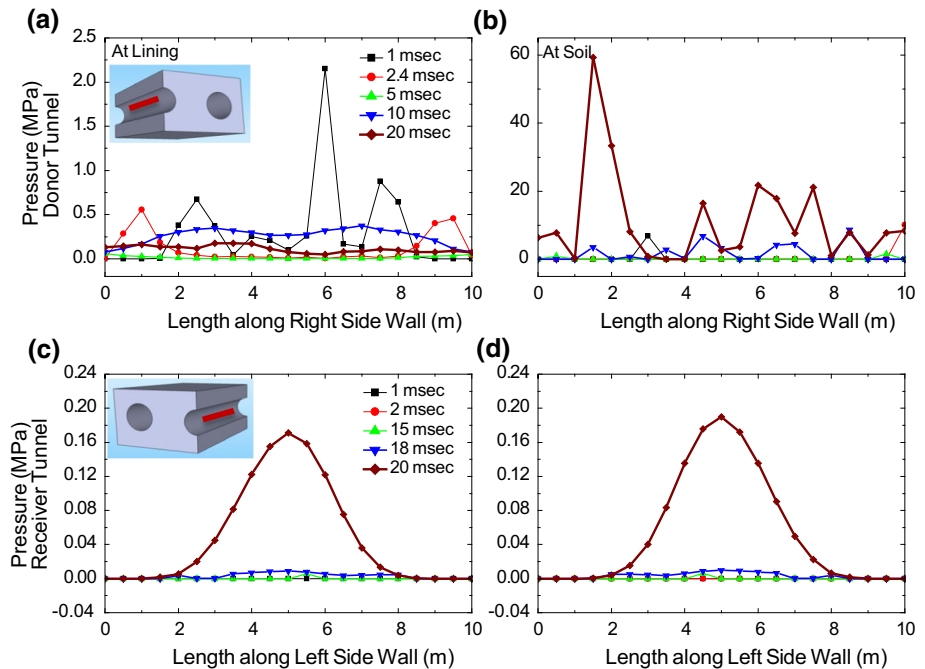Fig. 9 Displacement (y direction) in soil at 26 ms

Fig. 10 Deformation in twin tunnels at 26 ms

lining increases from tunnel crown to ground level up to a distance of 900 mm. Beyond 900 mm, the displacement of soil decreases towards the ground level. Almost similar displacement pattern is observed in the soil column

between the donor and receiver tunnel. Figure 10 shows the displacement contours in the soil at 26 ms. Higher deformation of the soil is observed near to the donor tunnel. Deformation in the soil decreases towards the receiver tunnel due to attenuation of shock wave and particle rearrangement.

Figure 11 shows the pressure in the RC lining and surrounding soil at different time instances. Figure 11a, b show the pressure in the donor tunnel, along the defined path in the RC lining and surrounding soil. Higher pressure is observed in the RC lining and surrounding soil of the donor tunnel. In case of RC lining of the donor tunnel, peak blast pressure (2.1 MPa) is generated at time instance 1 ms and gradually decreases with time. In soil surrounding the donor tunnel, however, higher pressure is observed which increases with increasing time due to propagation of shock wave in donor tunnel and damage of RC lining. Figure 11c, d show the pressure in the receiver tunnel at different time instances. Similar pattern of pressure is observed in the RC lining and surrounding soil of receiver tunnel. The shock wave propagates through the soil between the twin tunnels and generates peak blast pressure (0.18 MPa) in the RC lining of the receiver tunnel at the time instance 20 ms.

Design Recommendations

Blast resistant design of tunnels include increased tunnel lining thickness, use of steel fiber reinforced concrete panel, and shock absorbing material in tunnel lining [7]. Moreover, the soil domain surrounding the tunnel should

Fig. 11 Pressure in RC lining and surrounding soil at different time instances

be treated with suitable grout material in order to increase the yield strength of the material. For twin tunnels, the center to center distance of tunnels should be chosen through numerical analysis so that the effect of blast load in one tunnel does not propagate in the other tunnel. Also, proper ventilation should be provided in the tunnels to stop channeling of shock wave inside the tunnel.

Conclusions

Blast response of twin tunnels is investigated using 3-D nonlinear FE analyses when blast happens in one tunnel only. Explosion inside the donor tunnel is simulated using the coupled Eulerian Lagrangian analysis tool in finite element software Abaqus/Explicit. The soil and RC lining have been modeled using Lagrangian elements. The following conclusions are drawn:

1. Donor tunnel shows maximum displacement and damage in the RC lining and surrounding soil. Displacement in the RC lining and soil increase with time.
2. Receiver tunnel shows less pressure in the RC lining and surrounding soil, which may increase with increasing charge weight.
3. Displacement of soil surrounding the donor tunnel increases up to a certain distance from the RC lining and then gradually decreases.

References

1. Abaqus/Explicit User's Manual, version 6.11 (2011) Dassault Systèmes Simulia Corporation. Providence, Rhode Island
2. Al-Rub RKA, Kim SM (2010) Computational applications of a coupled plasticity-damage constitutive model for simulating plain concrete fracture. Eng Fract Mech 77:1577–1603
3. Bischoff PH, Perry SH (1991) Compressive behavior of concrete at high strain rates. Mater Struct 24:425–450
4. Carreira DJ, Chu K (1985) Stress strain relationship for plain concrete in compression. ACI J 82(6):797–804
5. Carreira DJ, Chu K (1986) Stress strain relationship for reinforced concrete in tension. ACI J 83(1):21–28
6. Chakraborty T, Larcher M, Gebbeken N (2013) Comparative performance of tunnel lining materials under blast loading. In: Proceedings of 3rd international conference on computational methods in tunneling and subsurface engineering, Ruhr University Bochum, Germany, 17th–19th April 2013
7. Chakraborty T, Larcher M, Gebbeken N (2014) Performance of tunnel lining materials under internal blast loading. Int J Prot Struct 5(1):83–96
8. Chille F, Sala A, Casadei F (1998) Containment of blast phenomena in underground electrical power plants. Adv Eng Softw 29(1):7–12
9. Choi S, Wang J, Munfakh G, Dwyre E (2006) 3-D nonlinear blast model analysis for underground structures. In: Proceedings of ASCE Geo-Congress 2006, Atlanta, Georgia, USA, 26th February–1st March 2006, pp 1–6
10. Design specifications. Delhi Metro Rail Corporation Limited, Barakhamba road, New Delhi, India
11. Dusenberry DO (2010) Handbook for blast resistant design of buildings, 1st edn. Wiley, Hoboken
12. Du H, Li Z (2009) Numerical analysis of dynamic behavior of RC slabs under blast loading. Trans Tianjin Univ 15(1):61–64
13. Feldgun VR, Kochetkov AV, Karinski YS, Yankelevsky DZ (2008) Internal blast loading in a buried lined tunnel. Int J Impact Eng 35(3):172–183
14. Feldgun VR, Kochetkov AV, Karinski YS, Yankelevsky DZ (2008) Blast response of a lined cavity in a porous saturated soil. Int J Impact Eng 35(9):953–966
15. Goel MD, Matsagar VA, Gupta AK, Marburg S (2012) An abridged review of blast wave parameters. Def Sci J 62(5):300–306
16. Gui MW, Chien MC (2006) Blast resistant analysis for a tunnel passing beneath Taipei Shongsan airport: a parametric study. Geotech Geol Eng 24:227–248
17. Higgins W, Chakraborty T, Basu D (2012) A high strain-rate constitutive model for sand and its application in finite element analysis of tunnels subjected to blast. Int J Numer Anal Methods Geomech 37(15):2590–2610
18. Johnson GR, Cook WH (1983) A constitutive model and data for metals subjected to large strains, high strain rates and high temperatures. In: Proceedings of 7th international symposium on ballistics, Hague, Netherlands, 19th–21st April 1983, pp 541–547
19. Karinski YS, Feldgun VR, Yankelevsky DZ (2008) Explosion-induced dynamic soil–structure interaction analysis with the coupled Godunov-variational difference approach. Int J Numer Methods Eng 77(6):824–851
20. Kumar M, Goel MD, Matsagar VA, Rao KS (2014) Response of semi-buried structures subjected to multiple blast loading considering soil-structure interaction. Indian Geotech J. doi:10.1007/s40098-014-0143-1
21. Larcher M, Casadei F (2010) Explosions in complex geometries—comparison of several approaches. European Commission, Joint Research Centre, Institute for Protection and Security of the Citizen, Italy
22. Lee J, Fenves GL (1998) Plastic damage model for cyclic loading of concrete structures. J Eng Mech 124(8):892–900
23. Lee JH, Salgado R (1999) Determination of pile base resistance in sands. J Geotech Geoenviron Eng, ASCE 125(8):673–683
24. Liu H (2011) Damage of cast-iron subway tunnels under internal explosions. In: Proceedings of ASCE Geo-Frontiers 2011, Dallas, Texas, USA, 13–16 March 2011, pp 1524–1533
25. Liu H (2009) Dynamic analysis of subway structures under blast loading. Geotech Geol Eng, ASCE 27(6):699–711
26. Lu Y (2005) Underground blast induced ground shock and it's modeling using artificial neural network. Comput Geotech 32:164–178
27. Lubliner J, Oliver J, Oller S, Onate E (1989) A plastic damage model for concrete. Int J Solids Struct 25(3):299–329
28. Ngo T, Mendis P, Gupta A, Ramsay J (2007) Blast loading and blast effects on structures: an overview. Electron J Struct Eng Spec Issue: Load Struct, 76–91
29. TM5-1300 (1990) Structures to resist the effects of accidental explosions. Technical Manual of the US Departments of the Army and Navy and the Air Force, USA
30. UFC 3-340-02 (2008) Structures to resist the effects of accidental explosions. Unified Facilities Criteria, US Departments of Army and Navy and Air Force, USA
31. Veyera GE, Ross CA (1995) High strain rate testing of unsaturated sands using a split-Hopkinson pressure bar. In: Proceedings of 3rd international conference on recent advances in

geotechnical earthquake engineering and soil dynamics, St.-Louis, Missouri, USA, pp 31–34

32. Yang Y, Xie X, Wang R (2010) Numerical simulation of dynamic response of operating metro tunnel induced by ground explosion. J Rock Mech Geotech Eng 2(4):373–384

33. Zhao CF, Chen JY (2013) Damage mechanics and mode of square reinforced concrete slab subjected to blast loading. Theor Appl Fract Mech 63–64:54–62